Local Field Controlled Switching in a One-Dimensional Dipolar Array

Jeroen J. de Jonge,[†] Mark A. Ratner,*[,†] and Simon W. de Leeuw[‡]

Department of Chemistry, Northwestern Univeristy, 2145 Sheridan Road, Evanston, Illinois, 60208, and Physical Chemistry and Molecular Thermodynamics, DelftChemTech, Delft University of Technology, Julianalaan 136, 2628 BL, Delft, The Netherlands

Received: July 31, 2006; In Final Form: October 30, 2006

We use computational Langevin dynamics simulations to show that the orientation of the dipolar rotors in a one-dimensional chain can be controlled using a local field. Flipping the direction of the field initiates a process in which each of the chain dipoles may switch its orientation. We define the conditions for which the dipole chain remains in one of its two stable orientations. We observe the switching mechanism between these two stable orientations using a local electric field generated by a fixed control dipole, and the effectiveness of the switching process as a function of temperature, rotational friction coefficient, length of the array, and magnitude of the control dipole. We show two examples of curved chains where this process is possible as well. We model molecular dipolar rotors as point dipoles and show that we can transfer a signal along a one-dimensional chain. The propagated signal is not a photon, phonon, or charge, but is rather mechanical. One could argue that this is the smallest array of mechanical gears.

1. Introduction

Molecular rotors have been discussed extensively.[1−3] Such rotors vary in size from a few angstroms to tens of nanometers, making them arguably the smallest rotors available today, and some of them are designed to be used as gears in nanoscale machines.[4−6] Rotors containing a dipole form an important subgroup, which is particularly interesting because the dipole−dipole interactions and the interactions with an external electric field can be used to control the orientation of the dipoles, and with that electrooptic and dielectric functions of materials.[7−9]

Figure 1 shows three dipolar rotors synthesized and characterized by the Colorado group and their collaborators (**1**,[10] **2**,[11] **3**[12]). These rotors differ in size, dipole moment, and geometry configuration. Rotor **2** is an azimuthal rotor that rotates parallel to the mounting surface. Rotor **3** is an altitudinal rotor attached to a surface with two stands on either side such that it rotates perpendicular to the surface. Rotor **1** is designed such that it can be placed in a sturdy three-dimensional grid.[10,13] Molecular dynamics simulations have shown that these particular rotors can show unidirectional motion when placed in an rotating electric field.[11−13]

Developments in synthesizing three-dimensional construction sets as described in refs 13 and 14 and in feedback controlled lithography (FCL)[15] make it possible to create ordered arrays of these molecular dipolar rotors using three-dimensional grids and attaching them to surfaces.

Modeling these dipolar molecules as classical point dipoles allows us to do numerous complete molecular dynamics simulations on large systems. We have examined how energy and signal can be transferred along one-dimensional (1D) chains of rotating dipoles.[16−19] These signals are of a mechanical kind and therefore much slower than electronic signals. However, no charge is transferred in the process; it is purely mechanical.

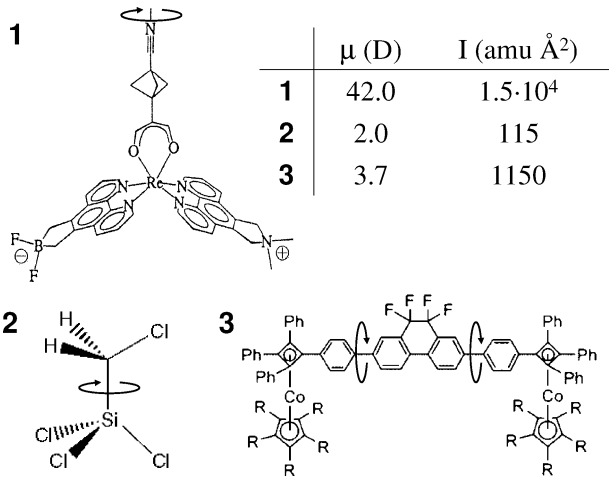

	μ (D)	I (amu Å^2)
1	42.0	$1.5\cdot10^4$
2	2.0	115
3	3.7	1150

Figure 1. Three dipolar rotors developed by the Michl group and collaborators (see refs 10−12) and their values for dipole moment μ and moment of inertia I (amu stands for atomic mass unit). The axes of rotation of the rotors are indicated by the arrows.

There has been strong interest in arrays of dipoles, both electric[20−22] and magnetic.[23−27] Ground states, and magnetization/polarization in external field and temperature, have been studied for ordered square, triangular, honeycomb, and rhombic lattices, theoretically for infinite systems[20−23] and computationally for finite systems.[24−27] Replacing the magnetic dipoles and field with electric ones should give identical results. Experimental results show the magnetization of 2D arrays of Co and Fe particles of different sizes and shapes in uniform magnetic fields.[28−31] In computational studies, uniform magnetic fields are usually employed.[23,24,26,27]

Here, we consider finite 1D chains of electric dipoles, all confined to rotate in the same plane (coplanar), and we investigate the orientation of the dipoles as a function of temperature and a local electrostatic field. Such dipole chains have two symmetric ground states at temperature zero, in which the dipoles line up nose-to-tail making an angle $\phi = 0,\pi$ with

* Corresponding author. E-mail: ratner@chem.northwestern.edu.
[†] Northwestern Univeristy.
[‡] Delft University of Technology.

10.1021/jp0648994 CCC: $37.00
Published on Web 02/08/2007

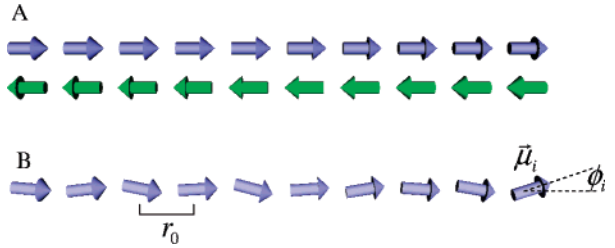

Figure 2. (A) Two symmetric ground states at zero temperature of a dipole chain: all of the dipoles align nose-to-tail in one direction, $\phi_i = 0$ in blue and $\phi_i = \pi$ in green. Temperature disrupts the ground state as the dipoles move. The cartoon (B) shows a typical configuration for low T, with dipole i making an angle ϕ_i with the chain axis.

the chain axis (Figure 2). (This ferromagnetic ordering of magnetic dipoles was observed experimentally for monoatomic chains of Co on a Pt substrate.[32]) For temperatures low compared to the interaction energy, the dipoles oscillate around one of the symmetric ground states. Applying a local nonuniform electric field breaks the symmetry and makes one nose-to-tail configuration energetically preferable to the other. In this paper, the source of the local electrostatic field is taken as a fixed control dipole, thus having an interaction with the dipoles proportional to r_i^{-3} where r_i is the distance between the control dipole and the ith dipole in the chain. (We refer to the dipole that provides the local field as the control dipole.) Only the dipoles close to the control dipole interact with it strongly; the dipoles further away have a weak interaction with the local field directly but "feel" the control dipole through the dipole−dipole interactions with the dipoles in between indirectly.

We use Langevin dynamics simulations to study the behavior of the dipoles in the chain as the control dipole's orientation is flipped. First, we examine the dynamics of the dipoles in the chain without the control dipole, determining the conditions for which the dipoles oscillate around the ground state (Section 3). In Section 4, the local field dipole is introduced and we monitor the behavior of the chain dipoles upon flipping the control dipole and the dependence of this process on temperature, number of dipoles, and the strength of the control dipole. This process also works for some nonlinear chains in Section 5. Finally, we summarize and discuss our results.

2. Langevin Dynamics Simulations

Langevin dynamics (LD) simulations are used to find the time evolution of the dipoles in the system. Compared to classical molecular dynamics (MD), Langevin dynamics includes two extra terms in the force calculations to model the friction and the temperature fluctuations. The dipoles are only allowed to rotate and not translate; therefore, the torque is calculated

$$I\frac{\ddot{\vec{\mu}}_i^{\mathrm{LD}}}{|\vec{\mu}_i|} = I\frac{\ddot{\vec{\mu}}_i^{\mathrm{MD}}}{|\vec{\mu}_i|} - \gamma I\frac{\dot{\vec{\mu}}_i}{|\vec{\mu}_i|} + \vec{R}_i \tag{1}$$

where $\ddot{\vec{\mu}}_i$ and $\dot{\vec{\mu}}_i$ are the second and first time derivatives of dipole moment i, I is the moment of inertia of the rotor, γ is the rotational friction coefficient, and $\vec{R}_i$ is a random term. The first term in eq 1, $I\ddot{\vec{\mu}}_i^{MD}$, comes from the interaction potential, the second term is the frictional term, and the last term sets the temperature for the system. If

$$\vec{R}_i = G_i\sqrt{\frac{2kT\gamma I}{h}}(\hat{\mu}_i \times \hat{n}) \tag{2}$$

then the temperature of the system is T.[34] In this expression, G_i is drawn from a Gaussian distribution, h is the time step size of the numerical integrator used in the calculations, $\hat{\mu}_i = (\vec{\mu}_i/|\vec{\mu}_i|)$ is the unit vector in the direction of $\vec{\mu}_i$, $\hat{n}$ is the unit vector perpendicular to the plane of rotation of $\vec{\mu}_i$, and k is the Boltzmann constant.

The dipoles in the system are subject to the dipole−dipole interactions

$$V_{ij} = \frac{1}{4\pi\epsilon_0}\left[\frac{\vec{\mu}_i\cdot\vec{\mu}_j}{r_{ij}^3} - 3\frac{(\vec{\mu}_i\cdot\vec{r}_{ij})(\vec{\mu}_j\cdot\vec{r}_{ij})}{r_{ij}^5}\right] \tag{3}$$

where $\vec{r}_{ij}$ is the center-to-center vector between dipoles i and j, and $r_{ij} = |\vec{r}_{ij}|$. Because each dipole has only one degree of freedom, the rotation angle ϕ_i, the dipole moment can be written as[19]

$$\vec{\mu}_i = \mu_i\mathbf{T}_i\cdot(\cos\phi_i, \sin\phi_i) \tag{4}$$

where μ_i is the size of the dipole moment and $\mathbf{T}_i$ is a transformation matrix (for a detailed description see ref 19). Because the only variable left is rotation angle ϕ_i, its time derivatives are are rotational velocity $\dot{\phi}_i$ and rotational acceleration $\ddot{\phi}_i$. The latter becomes the rotational force, or torque, multiplying it by the moment of inertia. The interaction torque $I\ddot{\phi}_i$ acting on the ith dipole can be written as[19]

$$I\ddot{\phi}_i^{\mathrm{MD}} = -\frac{1}{4\pi\epsilon_0}\sum_{j=1,i\neq j}^{N}\left[\frac{\vec{\mu}_i^T\cdot\vec{\mu}_j}{r_{ij}^3} - 3\frac{(\vec{\mu}_i^T\cdot\vec{r}_{ij})(\vec{\mu}_j\cdot\vec{r}_{ij})}{r_{ij}^5}\right] \tag{5}$$

where

$$\vec{\mu}_i^T = \frac{\mathrm{d}\vec{\mu}_i}{\mathrm{d}\phi_i} = \mu_i\mathbf{T}_i\cdot(-\sin\phi_i, \cos\phi_i) \tag{6}$$

is the vector perpendicular to $\vec{\mu}_i$ of the same size as $\vec{\mu}_i$. In this equation, $\vec{\mu}_i^T$, $\vec{\mu}_i$, and $\vec{\mu}_j$ only are time dependent through their angles ϕ_i and ϕ_j. The total torque (eq 1) now becomes in terms of ϕ_i

$$I\ddot{\phi}_i^{\mathrm{LD}} = I\ddot{\phi}_i^{\mathrm{MD}} - \gamma I\dot{\phi}_i + R_i \tag{7}$$

where the random R_i term now is a scalar:

$$R_i = G_i\sqrt{\frac{2kT\gamma I}{h}} \tag{8}$$

Starting with initial conditions for the dipoles at time $t = 0$, $\dot{\phi}_i(0)$ and $\phi_i(0)$, we numerically integrate $\ddot{\phi}_i^{\mathrm{LD}}$ from eq 7 according to the velocity Verlet scheme.[35]

In the computer calculations we use reduced units, which means that all quantities (temperature, energy, time) are written in units of dipole moment μ_0, the moment of inertia I_0, and the nearest neighbor distance r_0, thus becoming dimensionless. The real values of the quantities can be calculated from the reduced units using the real values for μ_0, I_0, and r_0

$$\mu = \mu^*\cdot\mu_0 \tag{9}$$

$$I = I^*\cdot I_0 \tag{10}$$

$$r = r^*\cdot r_0 \tag{11}$$

$$t = t^* \cdot t_0 = t^* \cdot \sqrt{\frac{4\pi\epsilon_0 I_0 r_0^3}{\mu_0^2}} \tag{12}$$

$$\gamma = \gamma^* \cdot \gamma_0 = \frac{\gamma^*}{t_0} \tag{13}$$

$$E = E^* \cdot E_0 = E^* \cdot \frac{\mu_0^2}{4\pi\epsilon_0 r_0^3} \tag{14}$$

in which Q^* is the quantity Q (where $Q = t, \gamma, E$) in reduced units and Q_0 is the real value of quantity Q per reduced unit, a function of μ_0, I_0, r_0, and physical constant $1/(4\pi\epsilon_0)$. The temperature is given in terms of the interaction energy E_0

$$T = T^* \cdot T_0 = T^* \cdot \frac{E_0}{k} \tag{15}$$

with k being the Boltzmann constant.

All of the quantities in this paper are presented in real units. For conversion we used $\mu_0 = 3.7$ D, and $I_0 = 1150$ amuÅ ^{2}, which are approximately the values for rotor **3**[36] in Figure 1, and a nearest neighbor spacing $r_0 = 20$ Å. Substituting these values in eqs 9−15, we find that $t_0 = 10.6$ ps, $\gamma_0 = 9.5$ ns^{-1}, $E_0 = 0.431$ kcal/mol, and $T_0 = 12.4$ K. The reduced temperature T^* is also often presented to compare temperature T with interaction energy E_0.

Because eq 7 has a random term R_i, the time evolution of a system is not unique. Instead, an ensemble of possible pathways exists; this is the essential characteristic of Langevin dynamics. For every system configuration, we average the results over 50 simulation runs. As initial configurations for these runs, we use uncorrelated configurations, taken from a simulation of an equilibrated configuration. When useful, the average values are presented with a sample standard deviation

$$s = \sqrt{\frac{1}{N_S}\sum_{n=1}^{N_S}(Q_n - \bar{Q})^2} \tag{16}$$

where Q_n is the calculated quantity from simulation run n, $\bar{Q}$ is its average, and N_S is the number of simulation runs (usually 50).

3. Dipole Chain

The two symmetric ground states, defined as the configurations with minimum potential energy at zero temperature, for a 1D dipole chain are the configurations in which the dipoles are perfectly lined up nose-to-tail (Figure 2A), pointing in one direction along the chain axis (blue), or in the exact opposite direction (green). At finite temperature T, the dipoles move according to (rotational) Brownian motion restricted by the interaction potential. The type of motion depends on the temperature.

Figure 3 plots the distribution $g(\phi)$ of the dipoles, which is the probability of a dipole having an angle with the chain axis ϕ at a certain time if the system is at a temperature T, for different temperatures T. Angle ϕ is calculated from the chain axis not distinguishing between the positive and negative direction. The data was acquired from 100 simulation runs, with the initial configurations split evenly over the two symmetric ground states. Note that the dipoles at the end of the chain have more freedom to rotate and their peaks are broader and wider than the peaks of the dipoles in the chain. This was also observed

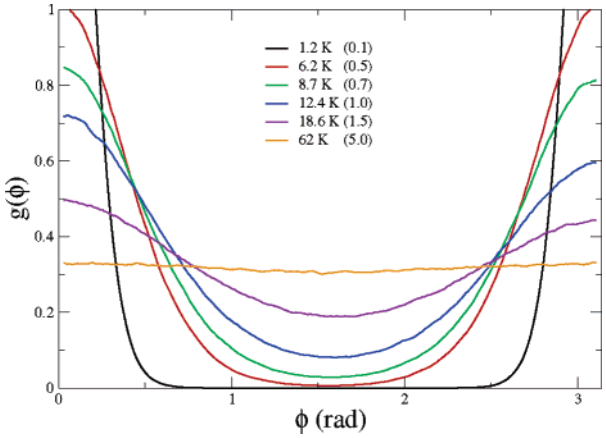

Figure 3. Normalized distribution function (top) of angles ϕ for different temperatures T. Reduced temperature T^* in brackets ($\gamma = 9.5$ ns^{-1}, $N = 10$).

for magnetic dipoles by Vindigni et al.[33] The distribution $g(\phi)$ is normalized such that $\int_0^\pi g(\phi)d\phi = 1$. For low temperatures compared to the interaction energy ($T = 1.2$, 6.2 K), the distribution $g(\phi)$ is nonzero only for angles around the ground states, $\phi = 0, \pi$. During the simulations with $T = 1.2$, 6.2 K, the dipoles only oscillated around their initial ground state. No half or full rotations are observed. At higher temperatures ($T =$ 8.7, 12.4 K), the dipoles mainly oscillate but also make (half) a rotation every now and then. Distribution $g(\phi)$ now has nonzero populations for $\phi = \pi/2$, although the populations are higher for $\phi = 0, \pi$. As temperature is increased to $T = 18.6$ K, the dipoles make rotations more often and the distribution becomes more evenly spread until at high temperatures ($T =$ 62 K) the distribution is uniform: the dipoles rotate stochastically according to Brownian motion, unhindered by the dipole−dipole interaction.

Examples of these three different behaviors are also shown in Figure 4, which plots the angular displacement $\varphi_i(t)$ of the dipoles for temperatures $T = 1.2$, 12.4, 64 K. φ_i are the accumulated angular rotations during the simulation. The three behaviors are clearly visible, from top to bottom: small oscillation, oscillation with occasional rotations, and stochastic rotation. In the middle graph the temperature is high enough that the dipoles are able to rotate, but not freely. Most of the time they oscillate around a stable orientation, and every now and then they make a half or full rotation, as is shown graphically by the jumps. The jumps are in arbitrary directions, and the dipoles at the end of the chain show a higher rate of jumps, which can be explained by the fact that their rotational potential wells are not as deep.

If the temperature is low enough such that the dipoles only oscillate, we say the system has a stable orientation: All of the dipoles point in the same direction and, although they fluctuate, they do not rotate to the opposite direction.

All of the results presented in this section are from systems with $N = 10$ dipoles and each dipole has a friction factor $\gamma = 9.5$ ns^{-1}. Calculations on systems with different friction coefficients, γ, or different chain lengths, N, resulted in similar qualitative and quantitative behavior.

4. Dipole Chain with Control Dipole

The addition of a local field, in our case a control dipole, on one side of the chain makes one stable orientation energetically more preferable than the other. The control dipole makes an

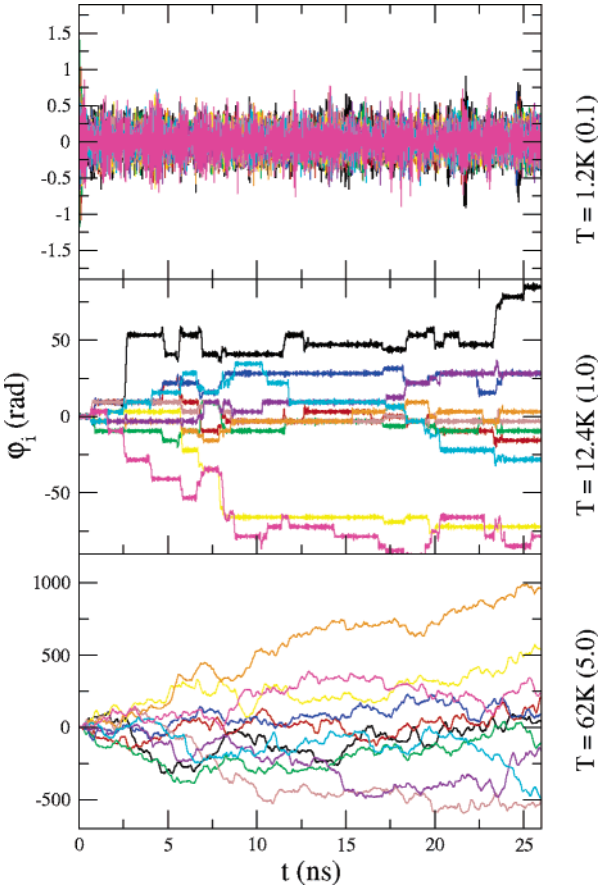

Figure 4. Angular displacements φ_i of the dipoles for $T = 1.2$, 12.4, 62 K (T^* in brackets) showing three different dynamical behaviors. The colors represent the different dipoles in the chain ($\gamma = 9.5$ ns^{-1}, $N = 10$).

angle ϕ_C with the chain axis and has a magnitude μ_C. In reduced units it is expressed in terms of μ_0:

$$\mu_C^* = \frac{\mu_C}{\mu_0} \tag{17}$$

If we control the direction of the control dipole ϕ_C, we may also control the orientation of the whole chain. The part that interests us is how the chain reacts to the change of the control dipole direction.

If the direction of the control dipole is switched from $\phi_C = 0$ to $\phi_C = \pi$ and if μ_C^* is large enough, then the dipoles that were in the stable orientation $\phi_i \approx 0$ will reorient themselves to $\phi_i \approx \pi$: they switch. For low temperatures, the reorientation of the dipoles in the chain occurs as a smooth process shown in Figure 5: At the moment the control dipole is switched ($t \approx 1$ ns), the first chain dipole immediately reacts and changes its orientation, followed by the second dipole, the third dipole, and so forth. The dipoles rotate over π radians in the opposite directions of their predecessor, similar to mechanical gears. The odd-numbered dipoles, plotted in black, rotate over $-\pi$ rad, and the even dipoles, plotted in brown, rotate over $+\pi$ rad. The switching of the dipoles propagates like a signal through the chain, where a dipole only switches after its predecessor has switched. The strong oscillation of the first dipole is due to the large amount of energy the dipole received upon the switching of the control dipole, and it takes some time to lose the energy through friction.

We now define the switch time, t_S, as the time it takes for the whole chain to reorient after flipping the control dipole. In

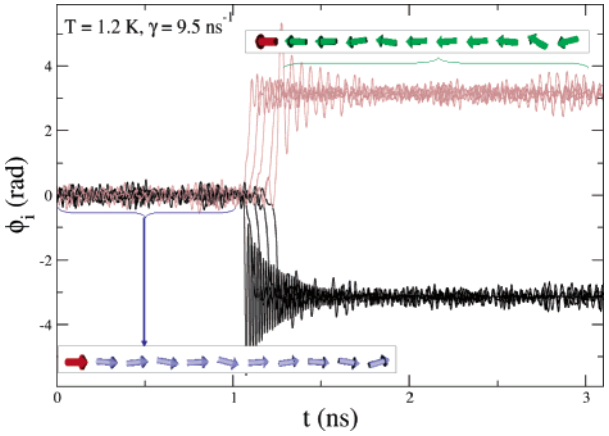

Figure 5. Time evolution of the chain dipole angles ϕ_i before and after switching the control dipole ($t \approx 1.0$ ns). The odd-numbered dipoles rotate π in the negative direction and are plotted in black, and the even numbered dipoles rotate π in the positive direction and are plotted in brown. The cartoons show the configurations of the chain in the two different stable configurations, before switching (blue) and after (green). The red dipole is the control dipole ($T = 1.2$ K (0.10), $\gamma = 9.5$ ns^{-1}, $\mu_C^* = 10.0$, $N = 10$).

Figure 5 we find $t_S \approx 200$ ps, and the dipoles switch in approximately equal time intervals (~20 ps). In the following sections, we examine the switch time t_S versus temperature T, friction coefficient γ, chain length N, and control dipole moment μ_C^*.

4.1. Switch Time versus Temperature and Friction. We calculate the switch times for different temperatures T and friction factors γ for a system of $N = 10$ dipoles. The result are plotted in Figure 6. The control dipole moment is chosen much larger than the chain dipoles, $\mu_C^* = 10.0$, and only temperatures in the oscillation range ($T < 6.2$ K) are considered. The presented values are averages over 50 simulations per combination of T,γ together with the standard deviation (eq 16). The graphs indicate that the average switch time increases with temperature and friction coefficient. This behavior is explained using two examples: Figure 7 plots the evolution of the chain dipoles, one for low T,γ (top) and one for high T,γ (bottom). For low temperatures and friction coefficients, the dipoles switch nicely one after another: the process is smooth and $t_S \approx 200$ ps. But, for high T,γ the rotational fluctuations of the dipoles are large, making the switching process more erratic and therefore increasing the switch time, $t_S \approx 500$ ps.

The erratic nature is also expressed by the larger spread in the values (larger error bars for high T,γ), indicating a more stochastic process for high T,γ.

4.2. Switch Time versus Chain Length. For a chain of 10 dipoles, we found that the switching process is smooth and regular at low temperatures and friction coefficients (Figure 5) and the switching of each dipole in the chain takes up approximately the same amount of time. One could make the assumption for low T that t_S is linear with the number of dipoles in the chain, N. However, simulations on systems with more dipoles show that this assumption is wrong. Figure 8 plots the average switch time versus the number of dipoles in the chain for three different temperatures and displays an exponential dependence of the switch time on the number of dipoles. The graphs are fit with an exponential curve of the form $t_S = t_S^0 e^{\beta(N-1)}$; see Table 1. For low temperatures, fitted values are very close to each other and the correlation is very close to 100%. Also, according to the error bars the spread of the

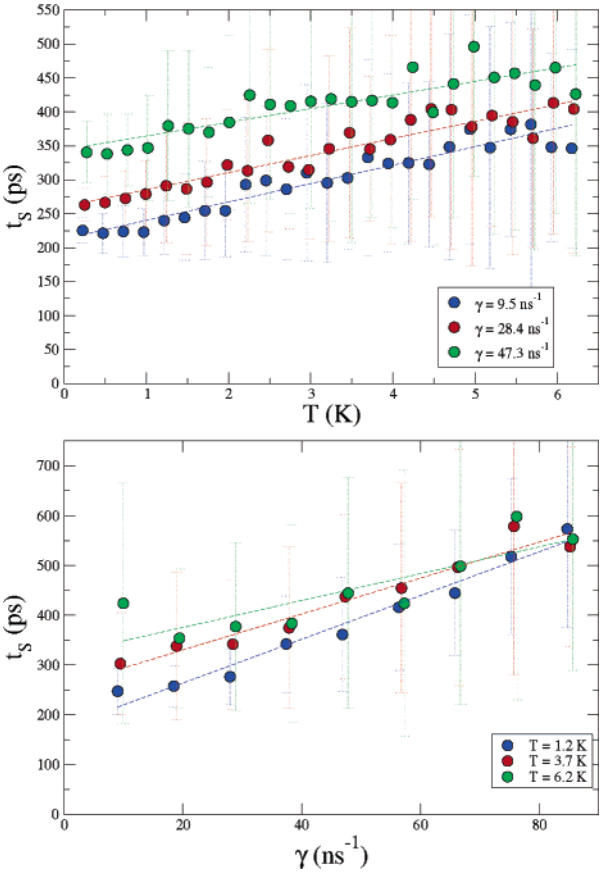

Figure 6. Average switch times t_S versus temperature T (top) and friction coefficient γ (bottom) ($N = 10$, $\mu_C^* = 10.0$).

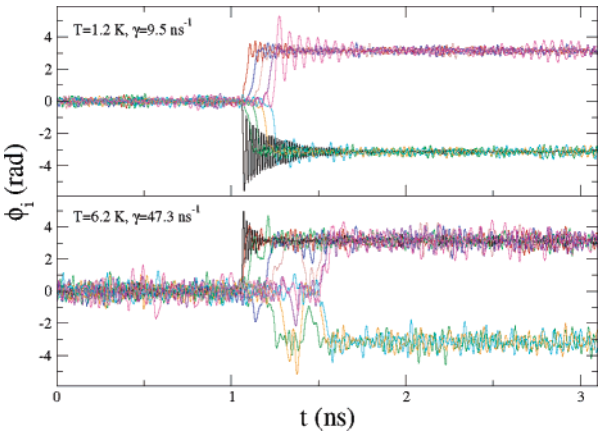

Figure 7. Time evolution of the chain dipole angles ϕ_i (each color represents one dipole in the chain) for a low temperature ($T = 1.2$ K (0.1), $\gamma = 9.5$ ns^{-1} top) and a high temperature ($T = 6.2$ K, $\gamma = 47.3$ ns^{-1} bottom) ($\mu_C^* = 10.0$, $N = 10$).

calculated values is very small. For $T = 1.2$ K the error bars are larger, especially for larger systems.

4.3. Switch Time versus Field Strength. All of the simulations above were done with a control dipole moment much larger than the chain dipole: $\mu_C^* = 10.0$. In this Section, we examine the dependence of the process on the size of the control dipole moment. We varied the control dipole moment between $1.0 \leq \mu_C^* \leq 15.0$ and calculated the switch times, t_S. Out of 50 simulations, the average values of t_S are plotted in Figure 9 together with the sample standard deviation (error bars). The switch time decays with increasing control dipole moment from $t_S > 600$ ps for $\mu_C^* = 2.0$ to $t_S \approx 230$ ps for $\mu_C^* > 8.0$. For small

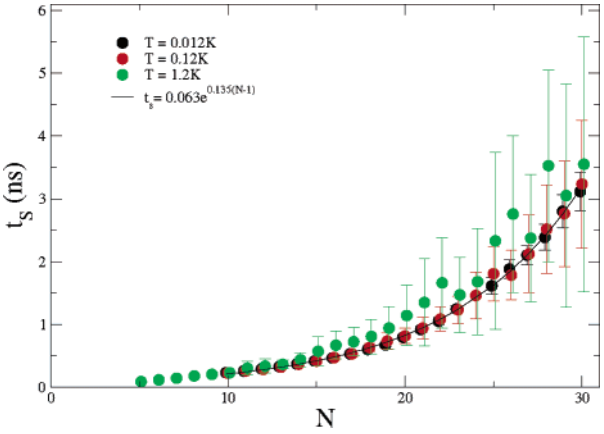

Figure 8. Average switch times t_S versus the number of dipoles in the chain N for three temperatures $T = 0.012$, 0.12, 1.2 K. The solid line presents the fitted exponential for $T = 0.012$ K ($\gamma = 9.5$ ns^{-1}, $\mu_C^* = 10.0$).

TABLE 1: Values for t_S^0 and β for the Exponential Fits of the Graphs of Figure 8[a]

T (K)	t_S^0 (ns)	b	corr (%)
0.012	0.063	0.135	99.97
0.12	0.064	0.135	99.85
1.2	0.107	0.122	98.4

[a] Corr is the correlation of the fitted values in percent.

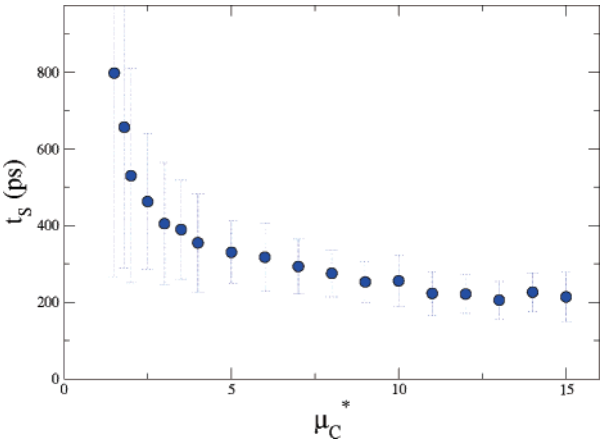

Figure 9. Switch time t_S versus control dipole moment μ_C^* ($T = 1.2$ K (0.1), $\gamma = 9.5$ ns^{-1}, $N = 10$).

values of μ_C^* the error bars are large, meaning that there is a big spread in the simulations. For some of the simulations with $\mu_C^* < 1.8$ the chains did not switch during the simulation run (~2 ns), and the results are not included in Figure 9.

The interaction of the control dipole with the first chain dipole is also influenced by the their distance, $r_{C,1}^*$, expressed in terms of the nearest neighbor distance r_0. From eq 3, the potential between the control dipole and the first dipole is proportional to

$$V_{C,1}\frac{\mu_C^* \mu_0^2}{(r_{C,1}^* r_0)^3} \tag{18}$$

meaning that a change in $r_{C,1}^* = X$ has the same result as a change for the dipole moment $\mu_C^* = X^{-3}$. It is possible to rewrite any combination of μ_C^* and $r_{C,1}^*$ with eq 18 to a single

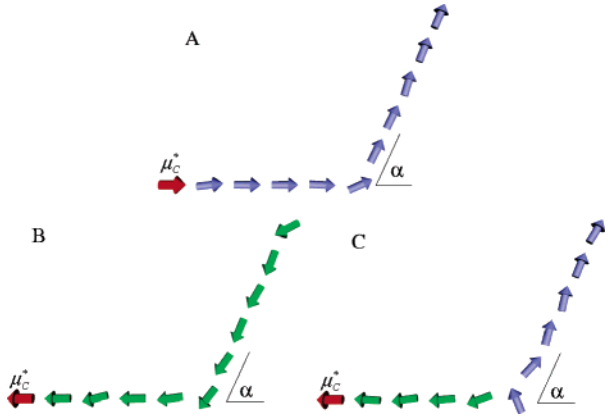

Figure 10. Cartoons of a chain with a kink α = 65° in its initial configuration (A), after a successful switch (B), and trapped in a local minimum (C).

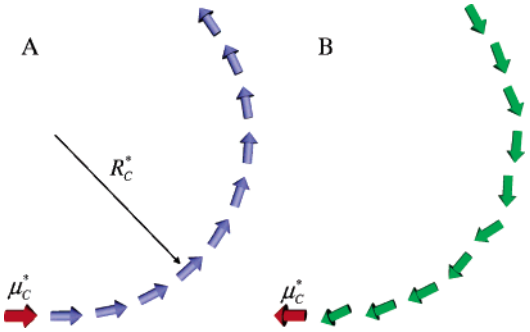

Figure 11. Cartoons of a circularly curved chain $R_C^* = 4.0$ (A) before and (B) substantially after switching the control dipole.

TABLE 2: Critical Temperature T_C ($T_C^* = 0.5$) for the Dipolar Rotors in Figure 1, with Varying r_0

	r_0 (Å)			
T_C (K)	15	20	30	50
rotor **1**			237	51
rotor **2**	4.3	1.8		
rotor **3**	14.7	6.2	1.8	

value for μ_C^*, for which the results are plotted in Figure 9, and therefore the dependence on distance $r_{C,1}^*$ will not be treated explicitly.

5. Nonlinear Chains

The switching process is not limited to perfectly linear chains. Simulations on chains with a kink (Figure 10) or circularly curved chains (Figure 11) also display switching behaviors depending on their geometries. The success of the switching process for the kink chain is limited by the angle α: Only for small angles α < 20° do the dipoles after the kink change their orientation. For angles α > 20°, the system can get stuck in a local minimum where the corner dipole has an angle $\phi_5 \approx (\pi - \alpha)/2$ (Figure 10C). The larger angle α, the bigger the chance that the switching process is halted.

The geometric limitations for the circular curved chain are defined by curvature radius R_C of the chain (Figure 11), defined in terms of inter-dipole distance $R_C^* = (R_C/r_0)$. Simulations on systems with different curvatures have shown that for chains with $R_C^* > 2.5$ the switching process is always successful and for radii $R_C^* < 2.5$ the process can get stuck in a local minimum. For a circular configuration, the angles between the sites can be approximated by angle $\alpha = R_C^{*-1}$ rad. In case $R_C = 2.5$, then α = 22°, which is equal to the angle we found for the kink above.

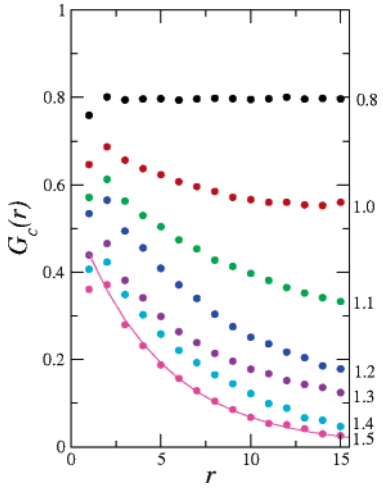

Figure 12. Correlation functions $G_c(r)$ for systems with different temperatures T^* (indicated on the right side of the graph). The solid line is the exponential fit according to eq 20. The systems were equilibrated at the temperatures, and the calculations were averaged over the middle 80 dipoles to avoid edge effects ($N = 100$ $\gamma = 9.5$ ns^{-1}).

6. Summary, Discussion, and Conclusions

For low temperatures, the dipole chain has two stable orientations. The critical temperature is estimated at $T_C = 6.2$ K ($T_C^* = 0.5$) for dipolar rotor **3** in Figure 1. If different dipole moments μ_0 or inter-dipole distances r_0 are used, then this value changes dramatically (see eq 15). Table 2 gives some combinations and their critical temperature showing that for rotors with large dipoles placed close enough to each other the critical temperature can be tuned to noncryogenic values.

If the conditions are such that the dipoles are in a stable orientation, then we can use a local electric field to control the orientation of the dipoles in the chain. Upon flipping the local control field (assumed to be at one end of the chain), the dipoles turn around one after the other in opposite directions, aligning with the new energetically preferable orientation. For low temperatures the process is smooth and takes ∼200 ps for a chain of $N = 10$ dipoles. For higher temperatures the switch time increases linearly, up to ∼500 ps for the critical temperature $T_C^* = 0.5$. The switch time is also linearly dependent on the rotational friction coefficient. The linear behavior is not valid for extreme value $\gamma = 0$ ns^{-1}; the dipoles have no friction, and therefore no energy will dissipate and the switching process does not occur as described. Another interesting case appears if $T = 0$ K. All dipoles are frozen and perfectly aligned, meaning that the interaction of the control dipole with the chain is theoretically zero, see eq 5. However, for the smallest disruption of this (theoretical), perfect alignment leads to a switch and a switch time t_S that is in agreement with Figure 6.

Another temperature-related issue is the correlation length. The same dipole orientations (to the left or the right, relative to the chain axis) can be observed only for a distance shorter than this temperature-dependent correlation length ξ, which means that in theory the orientational excitation can only be transferred over distances shorter than ξ. Correlation length ξ follows from the exponential decay of the spatial correlation $G_c(r)$

$$G_c(r) \sim e^{-r/\xi} \tag{19}$$

where r is the distance between two dipole sites. The correlation function $G_c(r)$ can be calculated from a system at a certain temperature T:

$$G_c(r) = \langle \vec{\mu}_i \cdot \vec{\mu}_j \rangle_t \text{ with } r = |r_i - r_j| \tag{20}$$

Figure 12 plots the $G_c(r)$ for systems with different temperatures T^*. The systems consisted of $N = 100$ dipoles, but only the middle 80 were taken into account for the calculation of eq 20. For systems with $T^* \geq 1.0$, an exponential decay can be observed for $r \geq 2$. These decays are comparable to correlation lengths of $\xi \approx 40$ for $T^* = 1.0$ and $\xi \approx 5$ for $T^* = 1.5$. For $T^* = 0.8$ no substantial exponential decay was observed, and a much longer correlation length $\xi \gg 40$ can be assumed for low temperatures because mostly a temperature $T^* = 0.1$ was used. Note that for neighboring dipoles $r = 1$ the correlation is a little bit lower than expected. This is because if one dipole has a positive angle, $\phi_i > 0$, then its neighboring dipole prefers to have a negative angle $\phi_{i\pm1} < 0$, resulting in a value for $G_c(r)$ much lower than expected according to eq 19.

The average switch time increases exponentially with the number of dipoles N, even for very low temperatures. This is in agreement with what was found earlier: coplanar dipoles have a non-acoustical dispersion curve,[16] and therefore there is a non-constant signal velocity resulting in a nonlinear but rather exponential growth of the switch time with N. The behavior is the same for low temperatures ($T = 0.12$, 0.012 K) and is not temperature-dependent in this regime; the error bars are small. For higher temperatures $T = 1.2$ K, looking at the error bars, the process becomes more erratic.

The magnitude of the control dipole plays an important role. The direct dipole−dipole interaction of the control dipole with dipole i in the chain decays with the distance according to r_{Ci}^{-3}. For the control dipole to have an interaction with the second dipole on the same scale as the neighbors of the second dipole, the dipole moment of the control dipole must be $r_{C2}^3 = 8$ times larger than chain dipole moments, and for the third dipole it needs to be 27 times larger. So, down the chain the direct influence of the control dipole is minimal. Now, assume that the switching process is at the 6th dipole. The interaction with the (already switched) 5th dipole is of equal strength as the interaction with the (unswitched) 7th dipole, and yet the 6th dipole switches its orientation to align with the 5th dipole (and the control dipole).

The following test was done to understand this behavior. We took a chain with the first half of the dipoles in the $\phi_i = \pi$ orientation and the second half with $\phi_i = 0$. Then, we ran simulations with and without a control dipole at $T^* = 0.1$. At the end of the simulation without the control dipole, about half the of the chain configurations were with $\phi_i \approx \pi$ for all of the dipoles and about half of the configurations with $\phi_i \approx 0$: No preference for any orientation was seen, as expected. If the control dipole was present ($\phi_C = \pi, \mu_C^* = 10.0$), then all configurations ended with $\phi_i \approx \pi$ for all of the dipoles. The switch times were all between $t_S = 106$ and 170 ps, varying from exactly half the time of a 10 dipole chain to 60% longer. In none of the cases did the signal first travel in the direction of the control dipole, but always away toward the end of the chain. So, although there is no direct influence of the control dipole on the dipoles down the chain, the control dipole has an indirect influence through the dipoles in between, hindering them to rotate in the opposite direction.

In all of our simulations the control dipole switched instantaneously. Simulations with a gradually rotating control dipole have not resulted in a smoother process or shorter switch times, validating the instantaneous switch used in our simulations.

We have shown that this switching process is not limited to perfectly linear chains; it also works in kinked chains and circular chains for certain geometries. For the chain with a kink, the angle should not be larger than $\alpha \approx 20°$, and for the circular chain the switching always works for radii larger than $R^* = 2.5$. We conclude that the switching mechanism works for dipole systems that have two stable orientations that can be accessed easily without getting stuck in local minima and if all of the interactions are of the same size. If, for instance, one of the dipoles in the chain has a much larger (or much smaller) dipole moment or a gap appears in the chain, then the process could be hindered or halted. If one would like to design logical circuits with these types of chains, then this should be taken into account.

Acknowledgment. This research was supported by the ARO under grant no DAAD19-01-1-0521 (DURINT) and by the NSF-MRSEC Program through the Northwestern MRSEC. We are grateful to J. Michl for helpful remarks.

References and Notes

(1) Gimzewski, J. K.; Joachim, C.; Schlittler, R. R.; Langlais, V.; Tang, H.; Johannsen, I. *Science* **1998**, *281*, 531−553.
(2) Dominguez, Z.; Khuong, T.-A. V.; Dang, H.; Sanrame, C. N.; Nunez, J. E.; Garcia-Garibay, M. A. *J. Am. Chem. Soc.* **2003**, *125*, 8827−8837.
(3) Kottas, G. S.; Clarke, L. I.; Horinek, D.; Michl, J. *Chem. Rev.* **2005**, *105*, 1281−1376.
(4) Balzani, V.; Credi, A.; Venturi, M. *Molecular Devices and Machines - A Journey into the Nano World;* Wiley: Weinheim, Germany, 2003.
(5) Stoddart, J. F. *Acc. Chem. Res.* **2001**, *36*, 410−411.
(6) Garcia-Garibay, M. A. *Proc. Natl. Acad. Sci.* **2005**, *102*, 10771−10776.
(7) Salech, B. E. A.; Teich, M. C. *Fundamentals of Photonics;* Wiley-Interscience: New York, 1991.
(8) Weber, M. J. *Handbook of Optical Materials;* CRC Press: Boca Raton, FL, 2002.
(9) Setian, L. *Applications in Electrooptics;* Prentice Hall: New York, 2001.
(10) Vacek, J.; Michl, J. *New J. Chem.* **1997**, *21*, 1259−1268.
(11) Clarke, L. I.; Horinek, D.; Kottas, G. S.; Varaska, N.; Magnera, T. F.; Hinderer, T. P.; Horansky, R. D.; Michl, J.; Price, J. C. *Nanotechnology* **2002**, *13*, 533−540.
(12) Zheng, X. L.; Mulcahy, M. E.; Horinek, D.; Galeotti, F.; Magnera, T. F.; Michl, J. *J. Am. Chem. Soc.* **2004**, *126*, 4540−4542.
(13) Vacek, J.; Michl, J. *Proc. Natl. Acad. Sci.* **2001**, *98*, 5481−5486.
(14) Schwab, P. F. H.; Noll, B. C.; Michl, J. *J. Org. Chem.* **2002**, *67*, 5476−5485.
(15) Hersam, M. C.; Guisinger, N. P.; Lyding, J. W. *J. Vac. Sci. Technol., A* **2000**, *18*, 1349−1353.
(16) de Leeuw, S. W.; Solvaeson, D.; Ratner, M. A.; Michl, J. *J. Phys. Chem. B* **1998**, *102*, 3876−3885.
(17) Sim, E.; Ratner, M. A.; de Leeuw, S. W. *J. Phys. Chem. B* **1999**, *103*, 8663−8670.
(18) de Jonge, J. J.; Ratner, M. A.; de Leeuw, S. W.; Simonis, R. O. *J. Phys. Chem. B* **2004**, *108*, 2666−2675.
(19) de Jonge, J. J.; Ratner, M. A.; de Leeuw, S. W.; Simonis, R. O. *J. Phys. Chem. B* **2006**, *110*, 442−446.
(20) Rozenbaum, V. M.; Ogenko, V. M.; Chuiko, A. A. *Sov. Phys. Usp.* **1992**, *34*, 88−902.
(21) Rozenbaum, V. M. *Phys. Rev. B* **1995**, *51*, 1290−1293.
(22) Rozenbaum, V. M. *Phys. Rev. B* **1996**, *53*, 6240−6254.
(23) Prakash, S.; Henley, C. L. *Phys. Rev. B* **1990**, *42*, 6574−6589.
(24) Stamps, R. L.; Camley, R. E. *Phys. Rev. B* **1999**, *60*, 11694−11699.
(25) Fazekas, S.; Kertesz, J.; Wolf, D. E. *Phys. Rev. E* **2003**, *68*, 041102.
(26) Takagaki, Y.; Ploog, K. H. *Phys. Rev. B* **2005**, *71*, 184439.
(27) Kayali, M. A.; Saslow, W. M. *Phys. Rev. B* **2004**, *70*, 174404.
(28) Hanson, M.; Johansson, C.; Nilsson, B.; Isberg, P.; Wappling, R. *J. Appl. Phys.* **1999**, *85*, 2793−2799.
(29) Kazakova, O.; Hanson, M.; Blomquist, P.; Wappling, R. *J. Appl. Phys.* **2001**, *90*, 2440−2446.

(30) Hanson, M.; Kazakova, O.; Blomquist, P.; Wappling, R.; Nilsson, B. *Phys. Rev. B* **2002**, *66*, 144419.
(31) Pulwey, R.; Zolfl, M.; Bayreuther, G.; Weiss, D. *J. Appl. Phys.* **2001**, *91*, 7995−7997.
(32) Gambardella, P.; Dallmeyer, A.; Maiti, K.; Malagoli, M. C.; Eberhardt, W.; Kern, K.; Carbone, C. *Nature* **2002**, *416*, 301−304.
(33) Vindigni, A.; Rettori, A.; Pini, M. G.; Carbone, C.; Gambardella, P. *Appl. Phys. A* **2006**, *82*, 385−394.
(34) Thijssen, J. M. *Computational Physics;* Cambridge University Press: Cambridge, U.K., 1999.
(35) Allen, M. P.; Tildesley, D. *Computer Simulations of Fluids;* Clarendon Press: 1987.
(36) Although rotor **3** is an altitudinal rotor, one can still arrange an array such that the dipoles rotate in the same plane, making the array coplanar.